Supplemental Information: Hyper-Raman spectroscopy of biological energy sources and chiral biomolecules

Christopher B. Marble,*[a] Kassie S. Marble,[a] Ethan B. Keene[b,c] Georgi I. Petrov,[b] and Vladislav V. Yakovlev[a,b,d].

a) Texas A&M University, Department of Physics and Astronomy, 4242 TAMU, College Station, TX 77843.

b) Texas A&M University, Department of Biomedical Engineering, 3120 TAMU, College Station, TX 77843.

c) Tarleton State University, Department of Chemistry, Geosciences, and Physics, 1333 W. Washington Stephenville, TX 76402.

d) Texas A&M University, Department of Electrical Engineering, 3127 TAMU, College Station, TX 77843.

Table of Contents

A. Validation of Experimental Design Using Pure Liquid Data S2

A.1 Dimethyl Sulfoxide S2

A.2 Methanol S4

A.3 Ethanol S5

B. Complete HRS Spectrum & Comparison of Reported Hyper-Raman, Raman, and IR Absorption Bands S7

B.1 D-Glucose S7

B.2 L-Arabinose S9

B.3 L-Alanine S11

B.4 L-Tartaric Acid S13

C. UV Absorption Cross-Sections for Liquids Analyzed S15

References S15

A | Validation of Experimental Design Using Pure Liquid Data

A.1 | Dimethyl Sulfoxide

Dimethyl sulfoxide (DMSO) belongs to the Cs point group (low symmetry group), meaning that all the 24 vibrational modes were expected to be IR, Raman, and hyper-Raman (HRS) active. At the low-frequency end of the experimental data, the bands observed in the Hyper Raman spectra from 305 cm^{-1} to 667 cm^{-1} were in great quantitative agreement with the bands observed in the Raman and infrared spectra. Two observed bands, the 900 cm^{-1}, and 934 cm^{-1} bands, were very weak in the hyper Raman spectra and were not reported in the Raman spectra of DMSO.[2] The S=O stretching region has been observed in both Raman and infrared spectra to be a convolution of several vibrational responses, likewise HRS cannot resolve the linewidths without deconvolution of features. Four H-C-H bending modes can be observed around 1290 cm^{-1}, 1310 cm^{-1}, 1411 cm^{-1}, and 1436 cm^{-1}; however, unlike the 1310 cm^{-1} and 1411 cm^{-1} bands, the band around 1290 cm^{-1} was seen only in HRS and IR. The 2914 cm^{-1} weak HRS band of DMSO corresponds to a peak observed in IR spectra. The C-H asymmetric stretching mode was reported by all three techniques to be around 2997 cm^{-1}. The full HRS spectra is provided as Fig. S1.

Comparing the depolarization ratio data from this experiment against the reported depolarization ratio $(\rho_{HR} = I_{HR\perp}/I_{HR||})$ data in Ref. 1, we find our reported values tend to trend higher on average than Ref. 1 (Table S1 with $> 2\sigma$ deviation bolded for emphasis). Furthermore, the reported depolarization ratio of the hyper-Rayleigh line was dramatically larger for our experiment. These differences may, in part, be a result of the near-resonant excitation of DMSO in our experiment (532 nm excitation), compared to Ref. 1 (1064 nm excitation experiment).

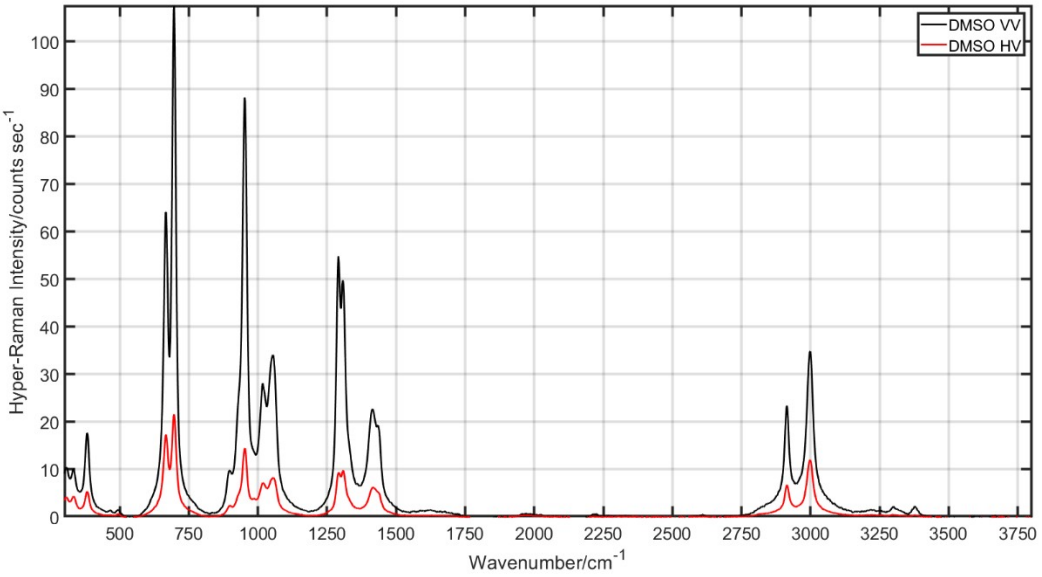

Fig. S1 The hyper-Raman spectra of DMSO for the VV and HV geometry are shown in black and red respectively post Savitzky-Golay filtering.

Table S1. Peak assignments for DMSO with their measured relative intensities, and depolarization ratios.

HRS (cm^{-1})*	Band Assignment[2, 3]	I_{Ratio} (x1000)	ρ	ρ[1]
0	Hyper-Rayleigh	1000 ± 30	**0.13 ± 0.01**	**0.45**
305	$\beta(C-S-C)$	9.4 ± 0.4	0.39 ± 0.02	0.35
334	$\beta_{out}(C-S=O)$	7.7 ± 0.3	**0.44 ± 0.02**	**0.23**
382	$\beta_{in}(C-S=O)$	12.3 ± 0.4	**0.317 ± 0.008**	**0.26**
667	$\nu_{Sym}(C-S)$	44 ± 1	0.288 ± 0.004	0.28
696	$\nu_{as}(C-S)$	63 ± 2	**0.225 ± 0.002**	**0.19**
900	Not Assigned	Very Weak		NR
934	Not Assigned	Very Weak		NR
955	$r(CH)$	61 ± 2	**0.170 ± 0.009**	**0.14**
1012	$r(CH)$	30 ± 1	0.27 ± 0.01	NR
1040-1060*	$\upsilon(S=O)$, υ (multiple)	41 ± 1	0.25 ± 0.008	NR
1290	$\beta(HCH)$	31 ± 1	**0.18 ± 0.01**	**0.13**
1310	$\beta(HCH)$	30 ± 1	0.20 ± 0.01	0.21
1411	$\beta(HCH)$	17.0 ± 0.7	0.261 ± 0.008	NR
1436	$\beta(HCH)$	12.6 ± 0.8	0.26 ± 0.02	NR
2914	$\upsilon_{sym}(CH)$	20 ± 1	0.30 ± 0.02	NR
2997	$\upsilon_{as}(CH)$	43 ± 3	0.34 ± 0.01	NR

*Where the uncertainty is unstated, it is +/- 1 cm^{-1}.

Abbreviations: sym=symmetry; as, asymmetric; ip, in-plane; out, out of plane; ν, stretching; β, bending; r, rocking

A.2 | Methanol

The HRS spectra and depolarization ratios of alcohols including methanol was previously reported by Ref. 4. The depolarization ratios and HRS spectra detected with our system was summarized and compared to the reported values for methanol (see Table S2). We find, in general, closer experimental agreement between our results and Ref. 4 than our DMSO results and Ref. 1 (see bolded entries in Table S2 for discrepancies).

As shown in Fig. S2 and Table S2, the high-wavenumber region of the HRS spectra of methanol was observed to contain the typical OH stretches (3200 cm^{-1} - 3600 cm^{-1}) and CH stretches of the CH_3 group was seen (2983 cm^{-1}, 2983 cm^{-1}, 2835 cm^{-1}) as were previously reported in literature. We report an additional, very weak, band around (2910 cm^{-1}) not previously reported for HRS in Ref. 4. The middle wavenumber range was also mostly characterized by the 1446 cm^{-1}, 1156 cm^{-1}, 1109 cm^{-1} bands which were identified as CH deformations and rocking motions of the CH_3 group. A strong peak observed around 1028 cm^{-1} was identified as a CO stretch. In the fingerprint regime, we observed one COH torsional peaks at 760 cm^{-1} and an O-H out-of-plane bending band at 630 cm^{-1} which were broadened via hydrogen bonding.

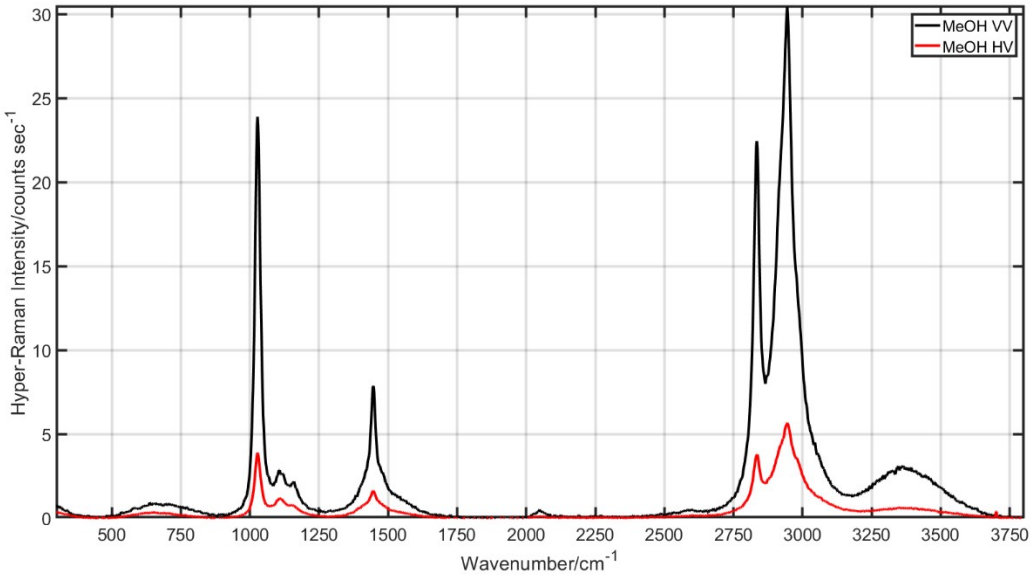

Fig. S2 The hyper-Raman spectra of methanol for the VV and HV geometry are shown in black and red respectively post Savitzky-Golay filtering.

Table S2. Peak assignments for methanol with relative intensities (to the hyper-Rayleigh line) and depolarization ratios.

HRS (cm^{-1})*	Band Assignment	I_{Ratio} (x1000)	ρ	ρ^4
0	Hyper-Rayleigh	1000 +/- 61	0.17 +/- 0.03	NR
630 (est.)	$\beta(COH)$	12 +/- 1	**0.40 +/- 0.04**	**0.6**
760	$\beta(OH)$ out-of-plane	8.4 +/- 0.8	0.19 +/- 0.03	NR
1028 +/- 1	$\nu(CO)$	58 +/- 4	0.17 +/- 0.03	0.17
1109 +/- 2	$r(CH_3)$	13 +/- 1	0.43 +/- 0.04	0.42
1156 +/- 2	$r(CH_3)$	8.3 +/- 0.6	**0.38 +/- 0.03**	**0.25**
1446 +/- 1	$def\ sym\ (CH_3)$	18 +/- 1	0.21 +/- 0.02	0.19
2835 +/- 1	$\upsilon_{sym}(CH_3)$	85 +/- 6	0.20 +/- 0.02	0.18
2910 +/- 3	NR	72 +/- 7	0.23 +/- 0.03	NR
2944 +/- 2	CH_3 (Fermi Resonance)	122 +/- 10	0.19 +/- 0.02	0.21
2983 +/- 2	$\upsilon_{as}(CH_3)$	59 +/- 5	0.28 +/- 0.03	NR
3200 -3600	$\upsilon(OH)$	Multi-Band	0.2 (est.)	0.15

*Where the uncertainty is unstated, it is +/- 1 cm^{-1}.

Abbreviations: sym, symmetry; as, asymmetric; ν, stretching; β, bending; r, rocking; def, deformation

A.3 | Ethanol

Ethanol, like methanol, has been previously studied using HRS.[4] As can be seen in Table S2, our depolarization ratios and observed HRS bands are in good agreement with the previously published results for ethanol (as can be seen in Table S2). The reported discrepancies at low wavenumbers may be in part, due to differences in our background subtraction methods for the ultrabroad response seen in hydrogen bonding liquids (see Ref. 3 supplement for our method applied to HRS of water where the background was a larger fraction of the total low wavenumber signal). Additionally, the bands we observe in the OH (3,125 cm^{-1} - 3,625 cm^{-1}) and CH (3,000 cm^{-1} – 2831cm^{-1}) stretching regions also agree with the previously observed spectra. Like water and methanol, we also observed a hydrogen bonding broadened response around 600 cm^{-1}. We report, but do not characterize some very weak responses that were observed around 2700 cm^{-1}, 2745 cm^{-1}, 2831 cm^{-1}.

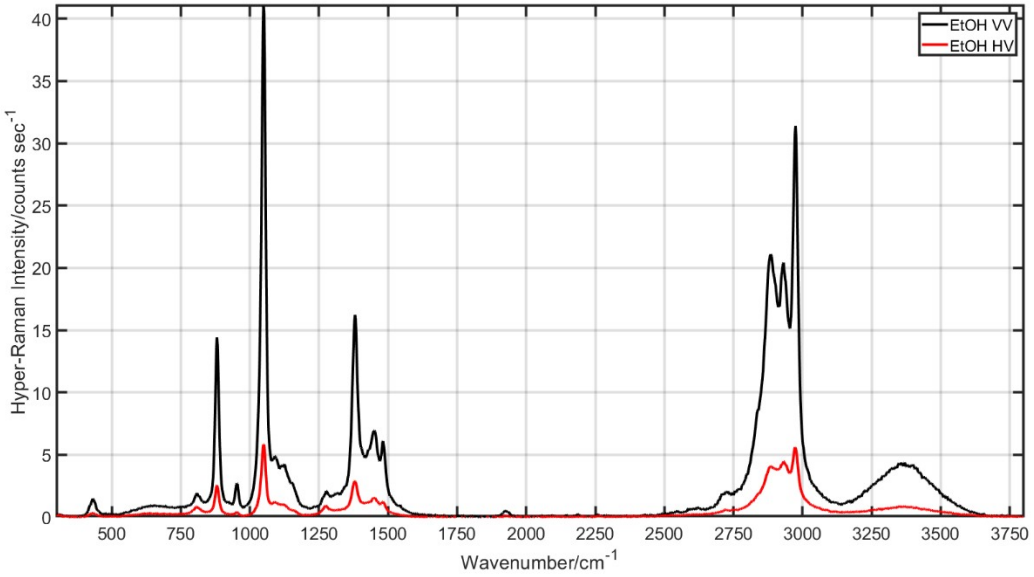

Fig. S3 The hyper-Raman spectra of ethanol for the VV and HV geometry are shown in black and red respectively post Savitzky-Golay filtering.

Table S3. Peak assignments for ethanol with relative intensities (to the hyper-Rayleigh line) and depolarization ratios.

HRS (cm^{-1})*	Band Assignment	I_{Ratio} (x1000)	ρ	ρ^4
0	Hyper-Rayleigh	1000 +/- 43	0.18 +/- 0.03	NA
432	$\beta(CCO)$	6.0 +/- 0.3	**0.23 +/- 0.02**	**0.27**
653 (est.)	$\beta(COH)$	NA	**~0.30**	**0.28**
810	$r(CH_2), r(CH_3)$	4.6 +/- 0.3	0.58 +/- 0.07	0.44
881	$\nu_{sym}(CCO)$	34 +/- 1	**0.18 +/- 0.01**	**0.21**
953	$r(CH_3)$	5.0 +/- 0.3	0.21 +/- 0.02	NR
1049	$\nu_{as}(CCO)$	124 +/- 5	**0.15 +/- 0.01**	**0.18**
1083 (est.)	$r(CH_3)$, COH def	NA	~0.24	0.23
1276	$\omega(CH_2)$	8.0 +/- 0.7	0.49 +/- 0.05	0.57
1381	$\omega(CH_2)$, Def sym (CH_3)	58 +/- 4	0.18 +/- 0.02	0.21
1448 +/- 2	Def as (CH_3)	39 +/- 3	0.23 +/- 0.02	0.25
1484	Def (CH_2)	16 +/- 1	0.22 +/- 0.03	0.19
2700 (est.)	NR	11 +/- 1	0.30 +/- 0.04	NR
2745 (est.)	NR	18 +/- 1	0.28 +/- 0.03	NR
2831 +/- 2	NR	31 +/- 2	0.22 +/- 0.03	NR

2883 +/- 2	$\nu_{sym}(CH_3)$	165 +/- 10	0.19 +/- 0.02	0.21
2933 +/- 2	$CH_3\ Fermi\ resonance$	148 +/- 10	0.23 +/- 0.03	0.28
2975	$\nu_{as}(CH_3)$	130 +/- 7	0.21 +/- 0.02	0.21
3361	$\nu(OH)$	197 +/- 8	0.23 +/- 0.02	0.19

*Where the uncertainty is unstated, it is +/- 1 cm^{-1}.

Abbreviations: sym=symmetry; as, asymmetric; ν, stretching; τ, twisting; ω, wagging; β, bending; r, rocking

B | Complete HRS Spectrum & Comparison of Reported Hyper-Raman, Raman, and IR Absorption Bands

In the following sections, we provide the full HRS spectra for each of the biomolecules presented in the article (Figs. 3-6 in the article show the spectra from 300 cm^{-1} to 1800 cm^{-1}).

B.1 | D-Glucose

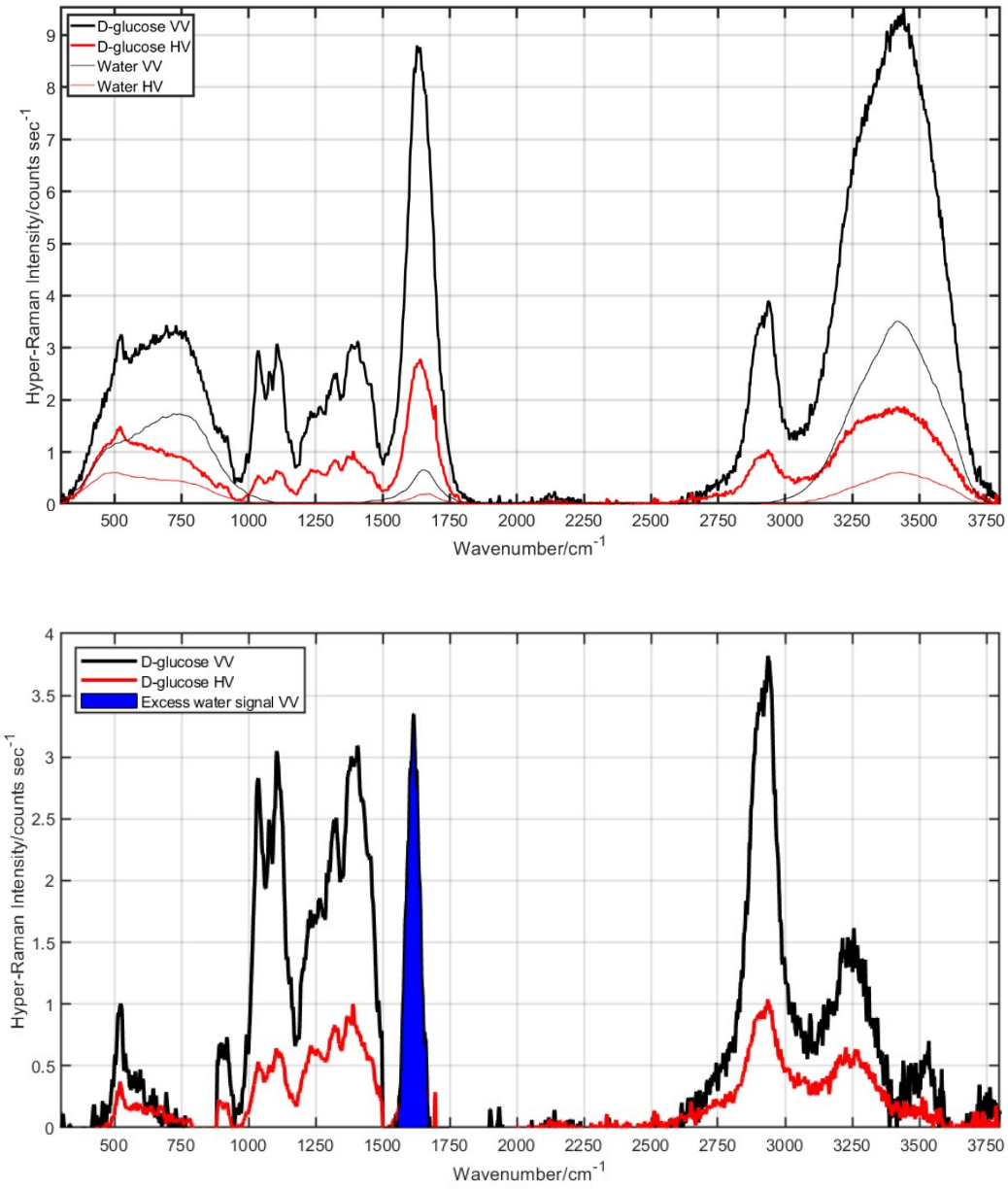

Fig. S4 (Top) The hyper-Raman spectra of D-glucose (in aqueous solution) for the VV and HV geometry are shown in black and red respectively post Savitzky-Golay filtering. Deionized water spectra under identical conditions are shown as thin lines. (Bottom) The hyper-Raman spectra of D-glucose (post-water subtraction) for the VV and HV geometry are shown in black and red respectively post Savitzky-Golay filtering.

Note in Fig. S4 bottom the presence of a false redshifted OH bend signal (~1615 cm^{-1}) from the water background.

Table S4. Comparison of D-glucose vibrational modes for HRS with Raman and infrared absorption.

Assignment	HRS (cm^{-1})*	RS[5] (cm^{-1})	IR[5] (cm^{-1})
Hyper-Rayleigh	0	0	NA
$\beta_{ip}(CCC)$,$\beta_{ip}(CCO)$,$\beta_{ip}(OCO)$	522	542	537
$\beta_{ip}(CCH)$,$\beta_{ip}(CCO)$	903 +/- 2	914	915
$\nu(CC)$,$\nu(CO)$, $\beta_{ip}(COH)$	1037	1022	1014
$\nu(CC)$,$\nu(CO)$, $\beta_{ip}(COH)$	1076	1074	NR
$\nu(CC)$,$\nu(CO)$, $\beta_{ip}(COH)$	1110 +/- 2	NR	1109
$\tau(CH_2)$	1248 +/- 2	NR	NR
$\omega(CH_2)$	1322 +/- 3	1333	1338
$\omega(CH_2)$	1386 +/- 2	1373	1371
$\delta(CH_2)$	1449 +/- 3	1460	1457
$\nu_{sym}(CH)$	2890 (est.)	2891	2891
$\nu_{Sym}(CH)$	2940 (est.)	2947	2943
$\nu_s(CH)$	2950 (est.)	2962	NR
$\nu(OH)$	3230 (est.)	3265	3296
$\nu(OH)$	3520 (est.)	NR	NR

*Where the uncertainty is unstated, it is +/- 1 cm^{-1}.

Abbreviations: sym=symmetry; as, asymmetric; ip, in-plane; ν, stretching; δ, scissoring; τ, twisting; ω, wagging; β, bending; r, rocking

B.2 | L-Arabinose

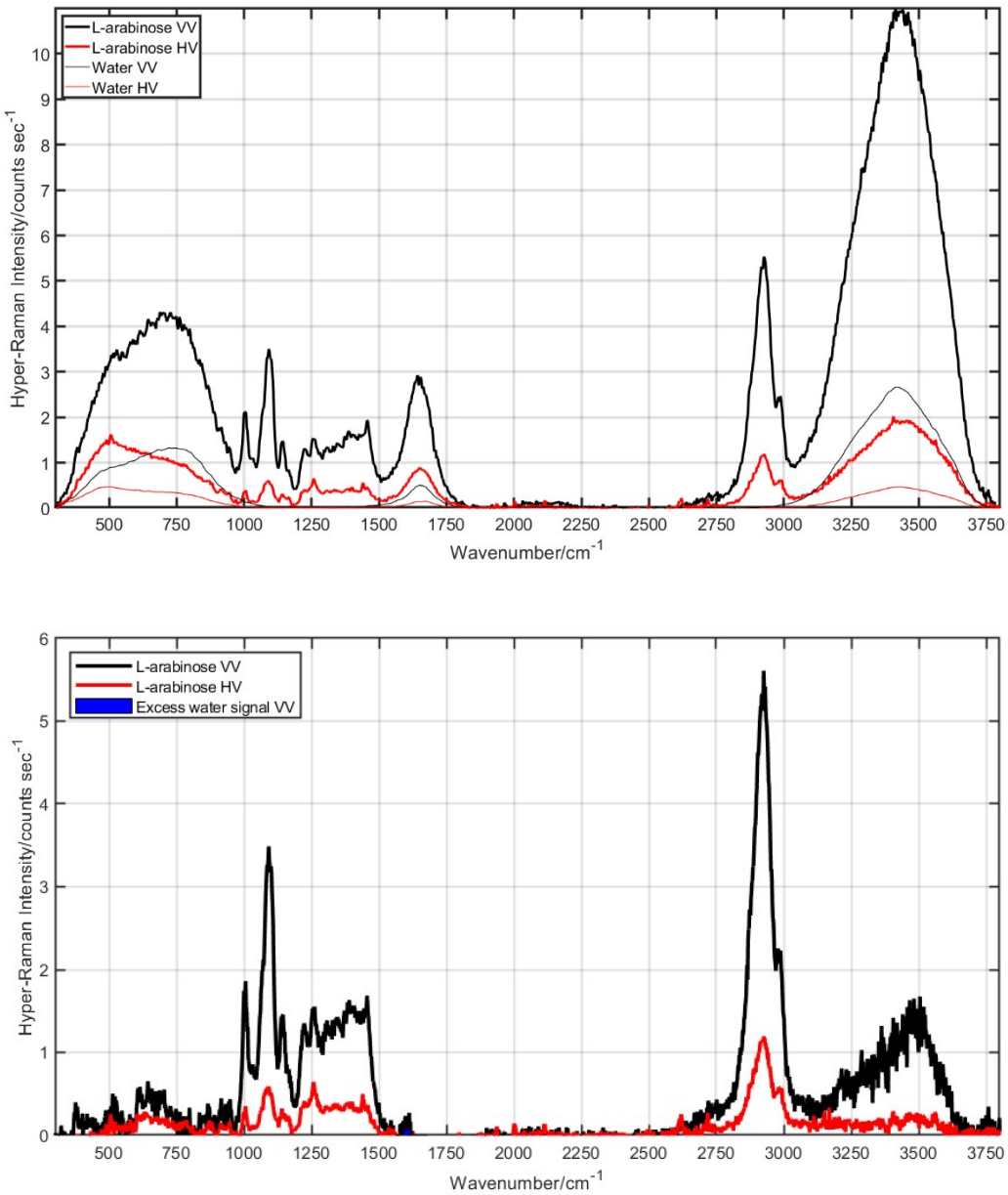

Fig. S5 (Top) The hyper-Raman spectra of L-arabinose (in aqueous solution) for the VV and HV geometry are shown in black and red respectively post Savitzky-Golay filtering. Deionized water spectra under identical conditions are shown as thin lines. (Bottom) The hyper-Raman spectra of L-arabinose (post-water subtraction) for the VV and HV geometry are shown in black and red respectively post Savitzky-Golay filtering.

Table S5. Comparison of L-arabinose vibrational modes for HRS with Raman and infrared absorption.

Band Assignment	HRS (cm^{-1})*	RS[5] (cm^{-1})	IR[5] (cm^{-1})
Hyper-Rayleigh	0	0	NA
$\beta_{ip}(COC)$	382	NR	399
$\beta_{ip}(COC)$	NR	430	431
$\beta_{ip}(CCC), ring\ def$	NR	NR	501
$\beta_{ip}(CCC)$, ring def	510	511	NR
$\beta_{ip}(CCC)$, ring def	577	579	578
$\beta_{ip}(OCO)$	612	612	602
$\beta_{ip}(OCO)$	645	NR	NR
$\beta_{ip}(OCO)$	700	698	NR
$\beta_{ip}(CH)$	872	897	891
$\beta_{ip}(CCH)$	919	928	NR
$\beta_{ip}(OCH)$	944	NR	942
$\nu_{as}(COC)$,$\nu(CC)$ $\beta_{ip}(CCH)$	1004	993	991
$\nu(CO)$,$\nu(CC)$ $\beta_{ip}(COH)$	1062 +/- 3	1051	1048
$\nu(CO)$	1094	1096	1089
$\nu(C-C)$	1145	1136	NR
$\tau(CH_2)$	1219	NR	1229
$\tau(CH_2)$	1259	1260	1256
$\omega(CH_2)$	1307	1312	1314
$\omega(CH_2)$	1345	1356	1354
$\omega(CH_2)$	1373	1375	1371
$\delta(CH_2)$	1450	1449, 1476	1473
$\nu_s(CH)$	2887	2891	2894

$\nu_s(CH_2)$	2929	2939	2938
$\nu(CH)$	2953	2959	2955
$\nu_{as}(CH)$	2976	2970	2967
$\nu_{as}(CH_2)$	3005	3001	2997
$\nu(OH)$	3100 - 3600	3337	3324, 3524

*Where the uncertainty is unstated, it is +/- 1 cm^{-1}.

Abbreviations: sym=symmetry; as, asymmetric; ν, stretching; τ, twisting; ω, wagging; β, bending; $\delta, scissoring$; r, rocking

B.3 | L-Alanine

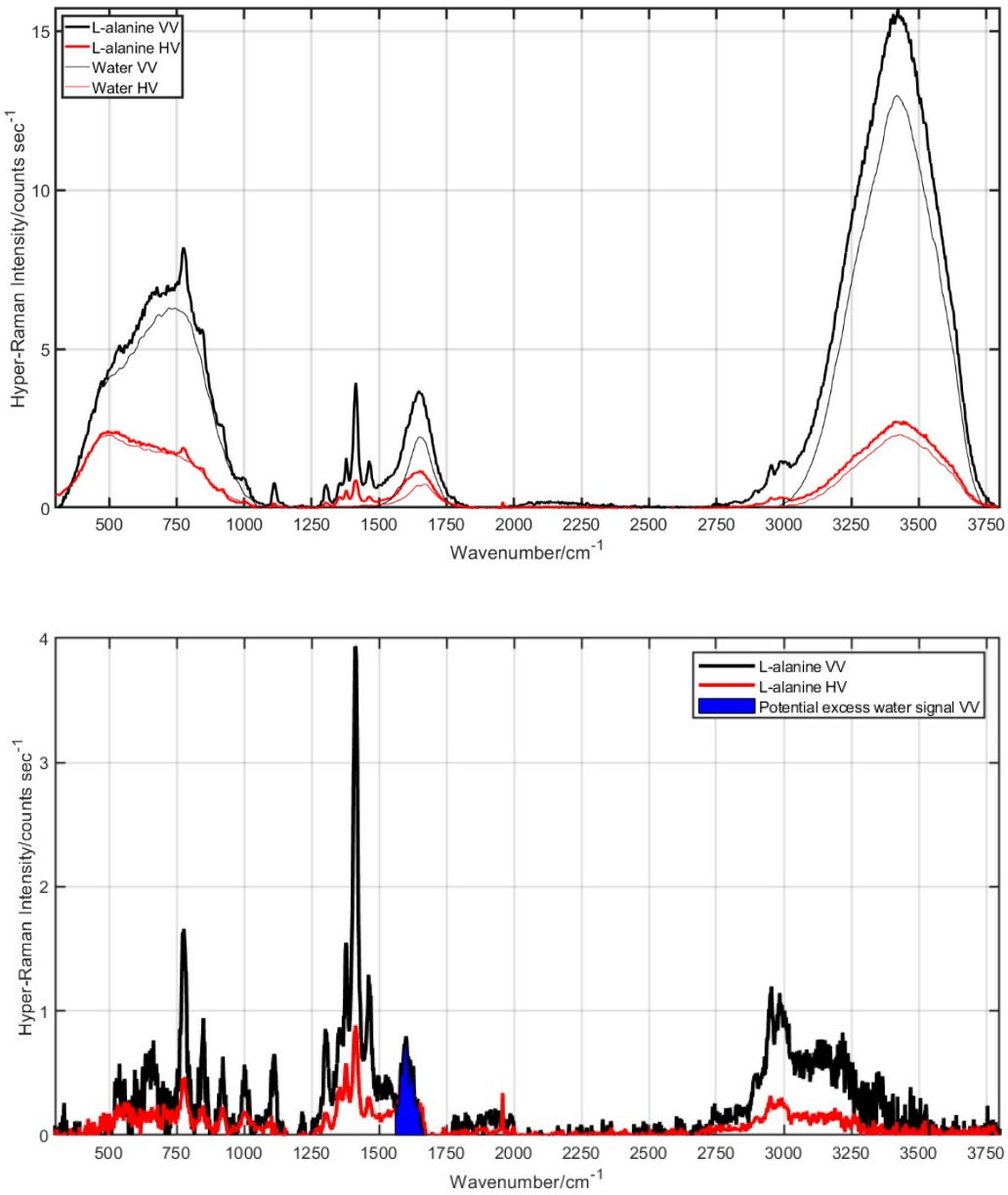

Fig. S6 (Top) The hyper-Raman spectra of L-alanine (in aqueous solution) for the VV and HV geometry are shown in black and red respectively post Savitzky-Golay filtering. Deionized water spectra under identical conditions are shown as thin lines. (Bottom) The hyper-Raman spectra of L-alanine (post-water subtraction) for the VV and HV geometry are shown in black and red respectively post Savitzky-Golay filtering.

Table S6. Comparison of L-alanine vibrational modes for HRS with Raman and infrared absorption.

Assignment	HRS (cm^{-1})*	RS[6,7] (cm^{-1})	IR[6,7] (cm^{-1})
$r(COO^-), \nu(CC), \delta(CCN), \nu(CN)$	541	553	544
$\delta(COO^-), \delta(CCN), \nu(CC), r(COO^-)$	648	654	646
$\omega(COO^-), \delta(CCC)$	777	781	769
$\delta(COO^-), \upsilon_s(COO^-), \nu(C-C)$ and $\nu(CN)$	847	862	851
$\nu(CN), r(CH_3), \nu(CC)$	920	930	919
$\nu(CC), r(CH_3)$	1005	1024	1014
$r(NH_3^+)$	1112	1125	1114
$\nu_{as}(CCN), r(CCN)$	1142 +/-2	1151	1149
$\nu_{sym}(CCO^-), r_{ip}(NH_3^+), r(CH)$	1304	1316	1307
$\delta(CH_3), \delta(NH_3^+)$	1353	1368	1354
$\delta_{as}(CH_3), \upsilon_{sym}(COO^-)$	1379	1388	1376
$\upsilon_{sym}(COO^-), \upsilon(CC), \delta_{as}(CH_3)$	1413	1423	1418
$\delta_{as}(CH_3)$	1462	1469	1462
$\delta_{sym}(NH_3)$	Very Weak	1527	1523
$\delta_{as}(NH_3)$	1600 (est.)	1604	1592
$rp(CH_3)$	2747 (est.)	2768	NR
$\nu_{sym}(CH_3)$	2899	2897	NR
$\nu(CH_3)$	2950	2960	2940
$\nu(CH_3)$	2984	2991	2982
$\nu(NH_3)$	3007	3011	3002
$\nu_{as}(NH_3)$	3093 +/- 7	NR	NR

*Where the uncertainty is unstated, it is +/- 1 cm^{-1}.

Abbreviations: sym=symmetry; as, asymmetric; ν, stretching; τ, twisting; ω, wagging; δ, scissoring; β, bending; r, rocking

B.4 | L-Tartaric Acid

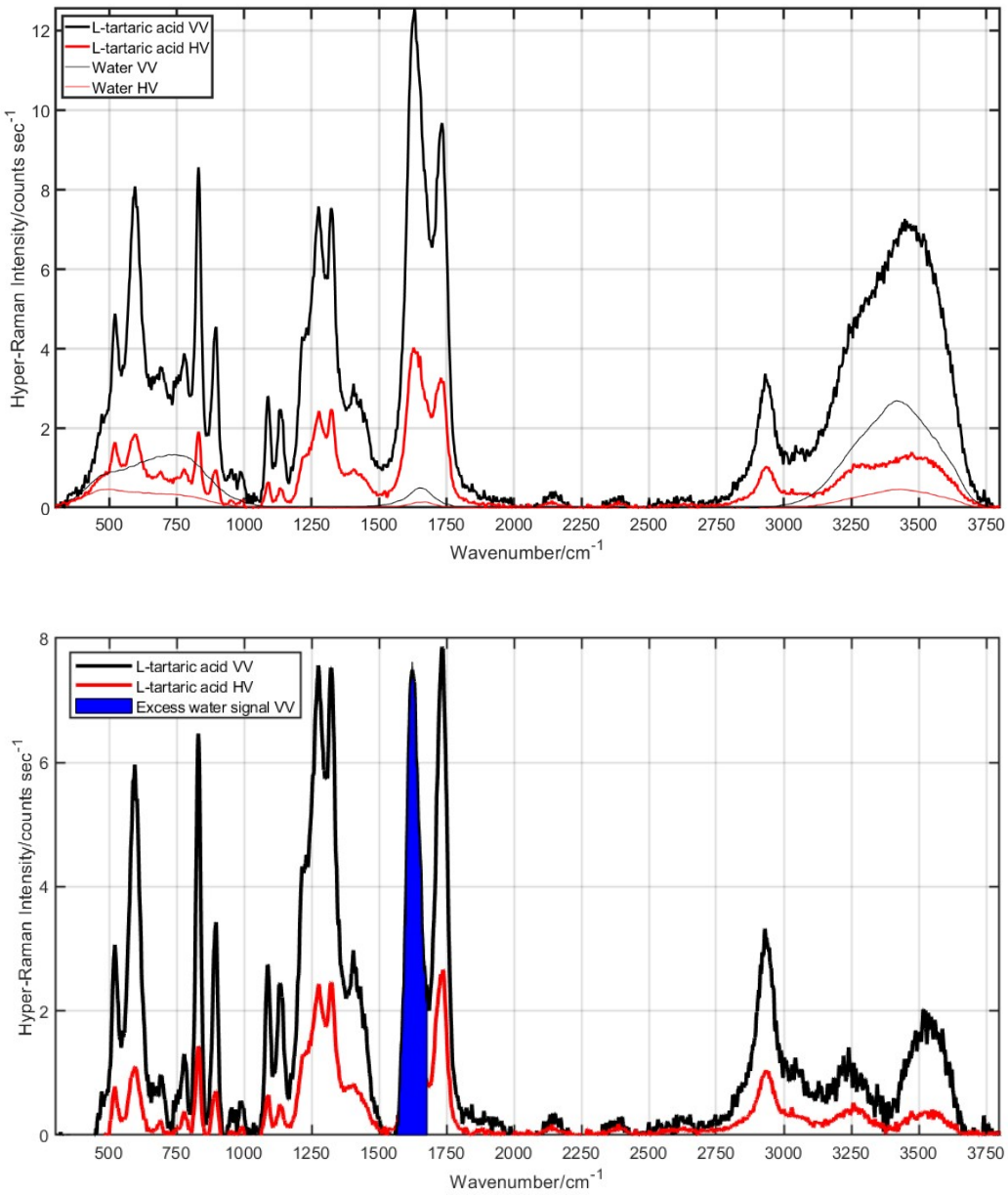

Fig. S7 (Top) The hyper-Raman spectra of L-tartaric acid (in aqueous solution) for the VV and HV geometry are shown in black and red respectively post Savitzky-Golay filtering. Deionized water spectra under identical conditions are shown as thin lines. (Bottom) The hyper-Raman spectra of L-tartaric acid (post-water subtraction) for the VV and HV geometry are shown in black and red respectively post Savitzky-Golay filtering.

Table S7. Comparison of L-tartaric acid vibrational modes for HRS with Raman and infrared absorption.

Assignment	HRS (cm^{-1})*	RS[8] (cm^{-1})	IR[8] (cm^{-1})
Hyper-Rayleigh	0	0	NA
$\tau(COOH)$	522	530	520
$\tau(COOH)$	595	582	580
$\tau(COOH)$	686	680	665
$\beta_{ip}(OCO), angle\ def$	778	758	790
$\beta_{ip}(OCO), angle\ def$	831	840	829
$\nu(C-C)$	NR	NR	873
$\nu(C-C)$	894	900	NR
$\nu(C-C)$	955	958	942
$\nu(C-C)$	992	996	992
$\nu(COH)$	1089	1090	1087
$\nu(COH)$	1136	1140	1134
$\beta_{ip}(C-H)$	1216 +/-2	1090	NR
$\beta_{ip}(C-H)$	1274 +/- 2	NR	1255
$\beta_{ip}(C-H)$	1328	NR	1318
$(COH)\ angle\ def$	1400 +/- 2,	1388	NR
$\nu(C-O)$	1459 +/- 2	NR	1453
$\nu(C=O)$	1730 +/- 2	1740	1741
$\nu(CH)$	2935	NR	2939
$\nu(OH)$	3230 (est.)	3176	3193
$\nu(OH)$	3540 (est.)	NR	NR

*Where the uncertainty is unstated, it is +/- 1 cm^{-1}.

Abbreviations: sym=symmetry; as, asymmetric; ν, stretching; τ, twisting; ω, wagging; β, bending; r, rocking

C | UV Absorption Cross-Sections for Liquids Analyzed

UV absorption spectroscopy was performed on all liquids using a Thermo Scientific GENESYS 10S UV-Vis spectrophotometer with a cuvette of distilled water as the calibration standard. The propagation distance of the HRS emission before exiting the cuvette is estimated to be 2 mm. The variation of UV transmission between 267 nm to 300 nm was 2% or less for all liquids except DMSO assuming a 2 mm path length for HRS light from the focal point to the cuvette wall (see Fig. S8).

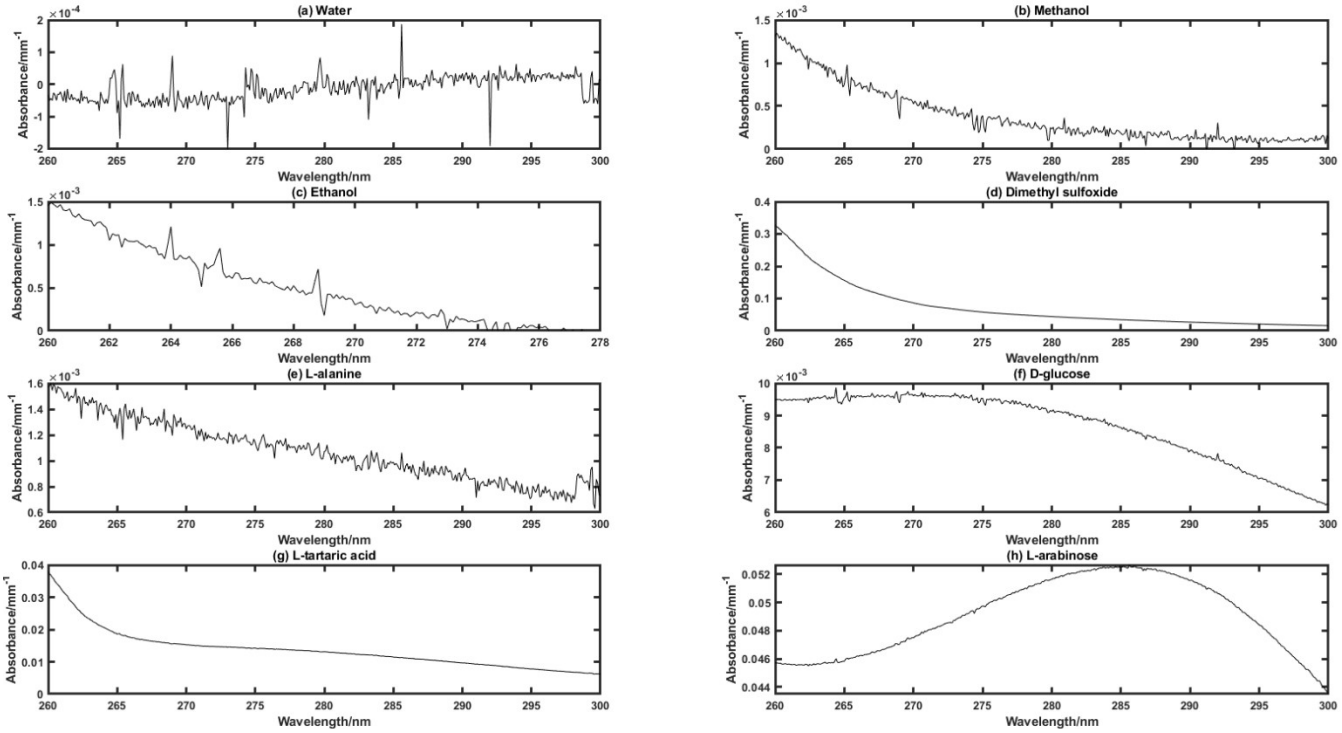

Fig. S8 The absorption spectra from 260 nm to 300 nm for all liquid samples studied at the concentrations used in the study.

References

1. M. Okuno, *J. of Chemical Physics*, 2020, **152**(17), 174202.
2. C. B. Marble, X. Xu, G. I. Petrov, D. Wang, V. V. Yakovlev, *Proc. SPIE 11656, Advanced Chemical Microscopy for Life Science and Translational Medicine 2021,* 2021.
3. C. B. Marble, X. Xu, G. I. Petrov, D. Wang, V. V. Yakovlev, *Phys. Chem. Chem. Phys.* 2021**, 23**, 24047-24051.
4. M. Okuno, *J. of Raman Spectroscopy*, 2021, **52**(4), 849-856.
5. E. Wiercigroch, E. Szafraniec, K. Czamara, M. Z. Pacia, K. Majzner, K. Kochan, A. Kaczor, M. Baranska, K. Malek, *Spectrochimica Acta - Part A: Molecular and Biomolecular Spectroscopy,* 2017, **185**, 317-335.
6. M. Túlio, S. Rosadoa, M. Leonor, R. S. Duarteb, R. Faustoc, *J. Molecular Structure*, 1997, **410-411**, 343-348.
7. S. Kumar, A. K. Rai, S. B. Rai, D. K. Rai, A. N. Singh, and V. B. Singh, *J. Molecular Structure*, 2006, **791**, 23-29.
8. R. Bhattacharjee, Y. S. Jain, and H. D. Bist, *J. Raman Spectroscopy,* 1989, **20**(2), 91-97.